ACS APPLIED MATERIALS & INTERFACES

Research Article

Cite This: ACS Appl. Mater. Interfaces 2019, 11, 16059−16064

www.acsami.org

Projection Printing of Ultrathin Structures with Nanoscale Thickness Control

Shangting You,[†] Wei Zhu,[†] Pengrui Wang,[‡] and Shaochen Chen*[,†,‡]

[†]Department of NanoEngineering, University of California San Diego, La Jolla, California 92093, United States

[‡]Material Science and Engineering, University of California San Diego, La Jolla, California 92093, United States

ABSTRACT: Spatial control of photon energy has been a central part of many light-based manufacturing processes. We report a direct projection printing method for ultrathin structures with nanoscale thickness control by using a patterned evanescent field. The evanescent field is induced by total internal reflection at the interface between the substrate and a prepolymer solution, and it is patterned by a phase-only spatial light modulator. The ultrathin structure is printed on a high-refractive-index glass substrate through photopolymerization. An iterative algorithm is used to calculate the phase pattern for generating arbitrary holography images and making the image plane to coincide with the interface. The thickness of the pattern is limited by the penetration depth of the evanescent field. Experiment results demonstrated that polymer structures as thin as 200 nm can be patterned without significant process optimization. Such fine control in thickness could transform many techniques such as light-based 3D printing and laser direct-write manufacturing.

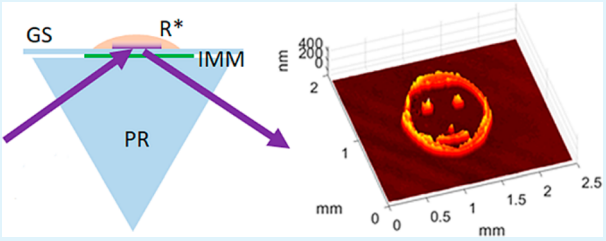

KEYWORDS: *evanescent field, total internal reflection, photopolymerization, holography, surface patterning*

INTRODUCTION

Light-based fabrication methods such as photolithography,[1] laser direct writing,[2,3] and light projection based 3D printing[4−6] have been playing significant roles in micro- and nanoscale 3D manufacturing in many industrial sectors. Among them, light projection based 3D printing which features fine fabrication resolution and extremely fast fabrication speed has attracted intense research interest.[7,8] The resolution of light projection based 3D printing in lateral direction is determined by the objective lens, which is typically a few micrometers,[9] and theoretically it can reach the diffraction limit, which is a few hundreds of nanometers. However, its fabrication resolution in the axial direction (along the light propagation direction) cannot match its lateral resolution. The typical axial resolution of light-based 3D printing method ranges from tens to hundreds of micrometers, depending on the material's light absorption property.[4]

When light propagates in an absorptive medium, it decays exponentially. The axial resolution of light-based 3D printing is determined by the light penetration depth in the photopolymerizable resin. Although doping highly light-absorptive additives does help to improve the axial resolution, the improvement is limited.[8] This has been a bottleneck for 3D printing of finer structures. To address this bottleneck, it is critical to limit the penetration depth of the patterned light field.

When light propagates from one medium to another, it can be partially reflected and partially refracted at the interface. If the first medium has a higher refractive index than the second medium, and the incident angle is greater than the critical angle, the light will be totally reflected back to the first medium. This phenomenon is well-known as total internal reflection (TIR).[10] Rigorous solution of Maxwell's equation of electromagnetic waves reveals that, though the light is totally reflected, a thin layer of electromagnetic field still exists in the second medium. This electromagnetic field, named as evanescent field, decays exponentially along the normal direction of the interface, and has a penetration depth at the scale of a wavelength.[10]

This thin evanescent field is very useful in some applications. For example, total internal reflection fluorescence microscopy (TIRFM)[11] uses the evanescent field to excite fluorescence from the specimen. The fluorescence signal comes only from a very thin layer, thus an ultrahigh signal-to-noise ratio can be achieved. Attenuated total reflection infrared spectroscopy (ATR−IR)[12] also uses the evanescent field to measure the infrared absorption spectrum of the samples.

The evanescent field can also be used for fabrication. Periodic patterns in photoresist have been fabricated by the interference of evanescent fields[13−16] or surface plasmonic waves.[17] Although ultrathin patterning can be achieved, arbitrary patterns cannot be generated by these multibeam interference methods. Metamaterials can be used to manipulate the light field and fabricate ultrathin arbitrary patterning.[18,19] However, using metamaterials will significantly increase the cost and complexity of the system. Laser direct writing technique employs a lens of high numerical aperture to focus the laser beam to achieve a fine resolution. However, the

Received: February 14, 2019
Accepted: April 9, 2019
Published: April 9, 2019

DOI: 10.1021/acsami.9b02728
ACS Appl. Mater. Interfaces 2019, 11, 16059−16064

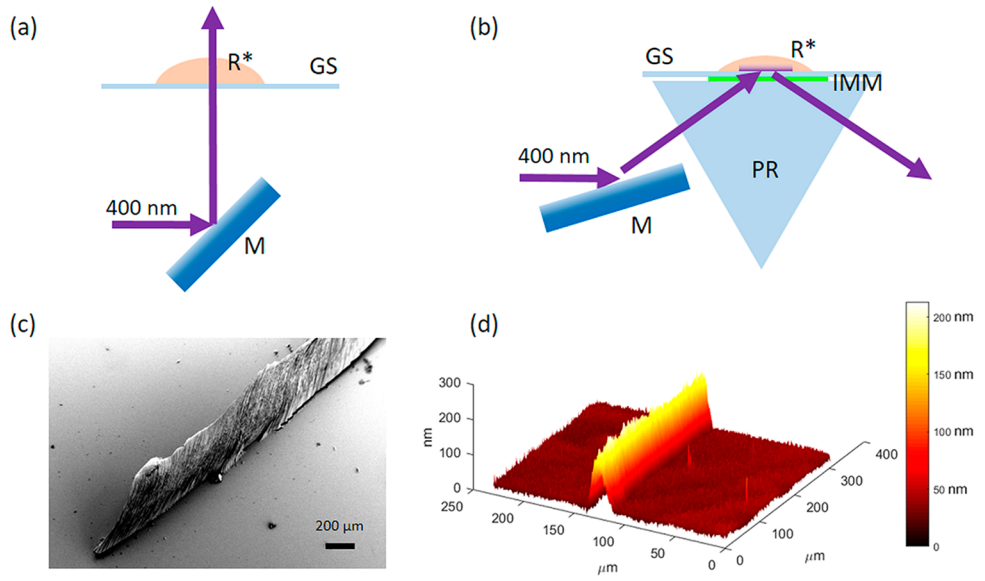

Figure 1. Comparison of the polymer pattern thickness between the propagating field and the evanescent field. (a) Schematic showing resin polymerized by the propagating field. (b) Schematic showing resin polymerized by the evanescent field. (c) SEM image of a structure polymerized by the propagating field. (d) Optical profiler image of a structure polymerized by the evanescent field. M: mirror, PR: prism, IMM: index-matched medium, GS: glass slide, R*: photopolymerizable resin.

point-scanning process is very time-consuming. Although ~50 nm lateral and ~20 nm axial resolutions has been achieved by femtosecond laser parallel scanning using microlens array on a phase-change film,[20] improvement in the fabrication speed is still limited. The fabricated pattern consists of array of small repeating patterns, and the use of phase-change film compromises the flexibility of this approach. Therefore, a flexible, cost-efficient approach for rapid fabrication of ultrathin arbitrary pattern is highly desired.

In this work, we show that the evanescent field can be patterned through a phase-only spatial light modulator (SLM) and projected to a prepolymer solution for direct printing of designed ultrathin structures. No physical mask is needed, and arbitrary patterns are produced with nanoscale thickness control in a projection fashion within a few seconds of exposure. The lateral resolution is theoretically limited by the diffraction limit. Because this setup requires a relatively long working distance, a high numerical aperture (NA) objective lens cannot be used. For the case of NA = 0.05, the lateral resolution limit is 4 μm. In our experiments, lens aberration dominates because we were using a spherical lens instead of an aberration-corrected lens, thus the lateral feature size we demonstrated is around 20 μm.

In order to make the image plane coincide with the TIR interface, the image plane cannot be perpendicular to the light incident direction. This tilted image plane is achieved by using holography technique to control the light distribution in 3D. To achieve good image quality and smooth intensity distribution, we adopt the mixed-region amplitude freedom (MRAF) algorithm[21] to generate an image in a tilted image plane. Various ultrathin patterns with arbitrary shapes are demonstrated.

RESULTS AND DISCUSSION

Polymerization Effect of Evanescent Field. In common light-based fabrication systems, light transmits through the prepolymer resin and gets attenuated exponentially inside the resin due to absorption, according to Beer–Lambert law. The penetration depth of the propagating light field is typically in the range of hundreds of micrometers to a few millimeters at near-ultraviolet (350 to 400 nm) wavelength.[22] For example, the 0.2% solution of a common photoinitiator, Irgacure 819, in ethonal has a absorbance of 3.0 cm^{-1}. Thus, the penetration depth of 1% Irgacure is calculated as 0.29 mm.

Total internal reflection creates an evanescent field, which decays exponentially. The penetration depth of the evanescent field is given by

$$d = \frac{\lambda}{4\pi}(n_1^2 \sin^2\theta_1 - n_2^2)^{-1/2} \quad (1)$$

where λ is the wavelength, n_1 and n_2 are the refractive indices of the two medias, and θ_1 is the incident angle.

Consider a situation where the refractive indices of the two mediums are 1.85 and 1.4, the wavelength is 400 nm, and the incident angle is 60°. Then the penetration depth of the evanescent field is 41 nm. Hence, direct patterning with nanoscale thickness control is possible to achieve.

We compared the photopolymerization effect between the propagating field and the evanescent field as shown in Figure 1. A 400 nm laser beam was modulated by a SLM and formed a line pattern at the interface between the glass slide and the photopolymerizable resin. Figure 1a shows a propagating field interacting with the resin, and Figure 1b shows an evanescent field interacting with the resin. The exposure time is 5 s for both cases. After exposure, we used isopropanol to remove the uncured resin. Both the glass slide and the equilateral triangular prism used in this experiment have a refractive index of 1.85 (N-SF11 glass). The index-matched medium couples the prism and the glass slide. The photosensitive resin is dipentaerythritol pentaacrylate (DPPA) with 1% Irgacure 819 as the photoinitiator. Figure 1c shows a scanning electron microscopy (SEM) image for the patterning result in case (a). Figure 1d is an optical profiler image showing the patterning results of case (b). The thickness of the polymer pattern polymerized by the propagating field is around 500 μm, and in

DOI: 10.1021/acsami.9b02728
ACS Appl. Mater. Interfaces 2019, 11, 16059–16064

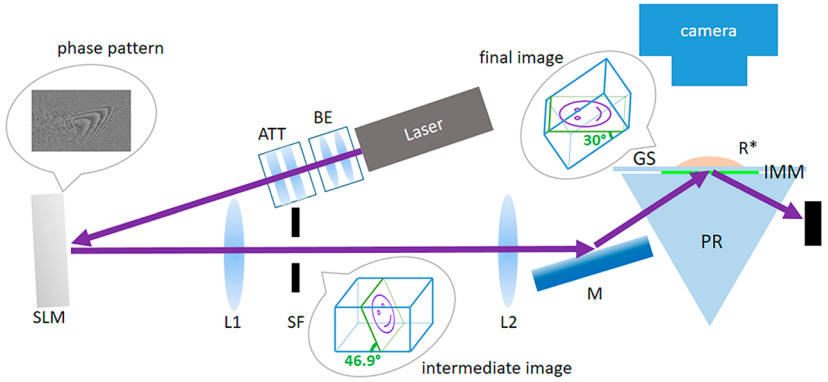

Figure 2. Optical setup of the ultrathin surface patterning system. BE: beam expander; ATT: attenuator; SLM: spatial light modulator; L1: lens 1; SF: spatial filter; L2: lens 2; M: mirror; PR: equilateral prism; IMM: index-matched medium; GS: glass slide; R*: photopolymerizable resin.

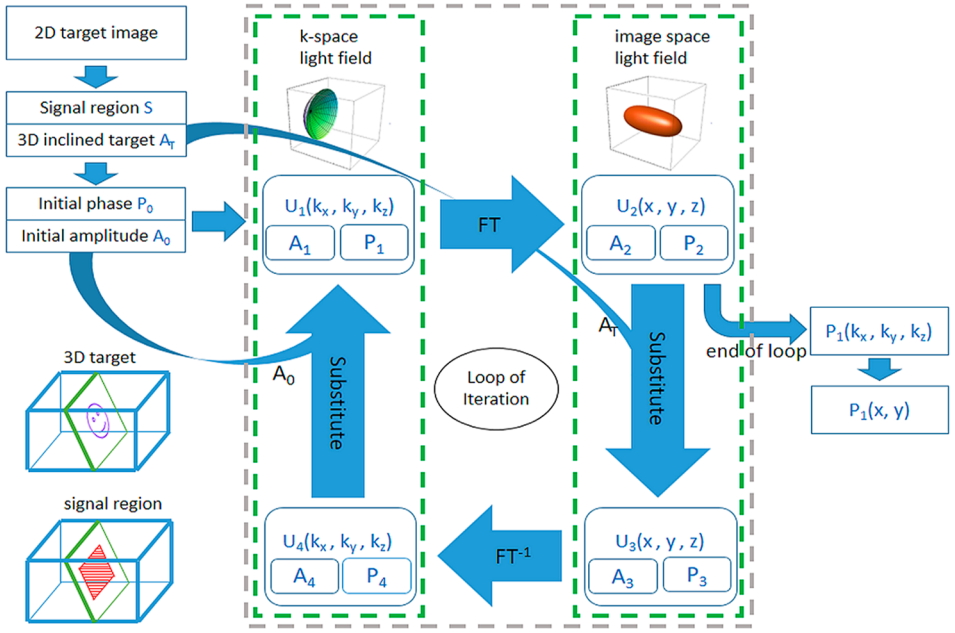

Figure 3. Block diagram of the 3D-MRAF algorithm.

comparison, the thickness of the polymer pattern polymerized by the evanescent field is only around 200 nm.

Direct Printing System Setup. The experimental setup of the ultrathin surface patterning system is shown in Figure 2. An ultraviolet laser beam (400 nm, 50 mW) passes through a beam expander and a tunable attenuator, and is modulated by the phase-only SLM. The phase pattern is loaded into the SLM so that the holographic image (intermediate image) can be found near the back focal point of lens *L1*. A diaphragm serves as a spatial filter which only allows the first order diffraction image to pass through. Lens *L2* is used to convert the intermediate image to the final image at 1:1 ratio. A mirror is used to redirect the beam so that it passes the prism at a normal incident angle. The equilateral prism is coupled with a glass slide by an index-matched medium. The laser beam irradiates the top surface of the glass slide at an incident angle of 60°, which leads to TIR. The prepolymer solution on the glass slide is polymerized by the evanescent field from the TIR. A camera is setup above the glass slide to collect the fluorescence excited by evanescent field and to help focusing the final image on the top surface of the glass slide. Note that by using the holography method, the intermediate image is tilted by 43.1° (namely, making a 46.9° angle to the light propagation direction), and the final image is tilted by 60° (namely, making a 30° angle to the light propagation direction). Therefore, the final image coincides with the top surface of the glass slide.

Both the equilateral prism and the glass slide is made of a high refractive index glass (N-SF11 glass, n = 1.85). An index-matched medium is used to couple the prism and the substrate. Diiodomethane (CH_2I_2) is one of the liquids with the highest known refractive index (n = 1.74),[23] hence it is selected to be the index-matched medium in this work.

The final image should be tilted by 60°. The prism's refractive index is 1.85 at 400 nm wavelength, under paraxial condition, the relation between the tilting angle of the virtual object δ_{obj} and the tilting angle of the final image δ_{img} is $\delta_{img}/\tan\delta_{obj} = n$. Thus, the virtual object of the final image should be tilted by 43.1°. Since lens *L2* images at 1:1 ratio, the intermediate image should also be tilted by 43.1°.

This tilted image plane can be achieved by using a tilted lens according to Scheimpflug principle,[24] or by using holography technique to control the light distribution in 3D. We found that a tilted standard spherical lens came with severe

DOI: 10.1021/acsami.9b02728
ACS Appl. Mater. Interfaces 2019, 11, 16059−16064

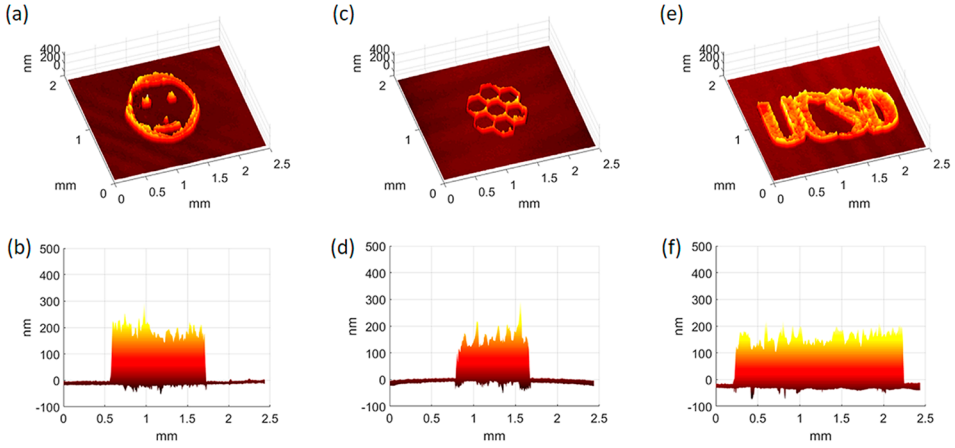

Figure 4. Optical profiler images of the patterned structure. (b), (d), and (f) are the side views of (a), (c), and (e), respectively. The thickness of these pattern is around 200 nm.

aberration, hence a specially designed tilted lens may be required. Therefore, we selected the holography method to tilt the image plane.

Holography Algorithm. Iterative Fourier transform algorithms such as Gerchberg−Saxton (GS) algorithm, adaptive-additive (AA) algorithm, and mixed-region amplitude freedom (MRAF) algorithm are commonly used in calculating the phase pattern in computer-generated holography (CGH).[21,25−29] Among those algorithms, GS algorithm and AA algorithm have shown their capability of shaping the light in 3D.[27,30] However, the intensity profile of the images generated by these algorithms is not smooth. Therefore, multiexposure by multiple frames of CGH are needed to smoothen the image and to avoid speckles.[31]

MRAF algorithm[21] can achieve better image quality and smoother intensity distribution than other iterative Fourier transform algorithms. Although the original MRAF algorithm can only be applied to creating 2D arbitrary images,[21] we modified this algorithm so that it is capable of controlling the light distribution in 3D. A 2D image in a tilted plane is fed into the 3D-MRAF algorithm as a 3D target image. The phase pattern can be calculated within half an hour by a common desktop computer.

The key idea of the MRAF algorithm is to divide the image space into a signal region and a noise region. In the signal region, phase freedom is allowed, and the intensity is restricted. In the noise region, both phase freedom and intensity freedom are allowed. In order to extend this idea into a 3D space, we make the 3D signal region as a single layer rectangular sheet (namely, 1 voxel thickness), which contains the target image, and coincides with the tilted image plane (see Figure 3: signal region). The rest of the voxels in the image space are noise region.

The schematic of 3D-MRAF algorithm is shown in Figure 3. The 3D inclined target image and 3D signal region are first determined according to the desired 2D target. Next, the initial amplitude on the SLM is set to 1 and the initial phase is set as a quadratic function, so that the resulting holography image is a square that covers the signal region.[21] Next, the light field on the SLM is converted into a 3D k-space, and all the nonzero voxels are on the Ewald's surface[27,32] (See Figure 3: k-space light field). Then it goes into the iteration.

The iteration is a loop among four complex light fields. Light field U_1 is a 3D light field in the k-space, where nonzero voxels are all on the Ewald's surface. U_1 represents the light field modulated by the SLM. Then the light field U_2 is acquired by applying a 3D Fourier transform to U_1.

Light field U_2 is the holography image of U_1 in image space. U_2 is converted to U_3 by substituting its amplitude with a mixture of its amplitude A_2 and the target A_T (eq 2). The mixing parameter β is 0 in the noise region, and is a number between 0 and 1 within the signal region.

$$\begin{cases} A_3 = \beta A_T + (1-\beta)A_2 \\ P_3 = P_2 \end{cases} \tag{2}$$

Then U_3 is converted to U_4 by applying an inverse Fourier transform.

Light field U_4 is not achievable by an SLM. Therefore, a physical restrain needs to be applied. The amplitude of voxels beyond the Ewald's surface are set to zero, and the amplitude of voxels within the Ewald's surface is set to the initial intensity A_0. The phase of all voxels remain unchanged. By this substitution, we get a new U_1.

This loop is repeated until the maximum count of iteration is met, or the error function between A_2 and A_T is smaller than the threshold. The phase of U_1 is converted back to the 2D space on the SLM: $P_1(x,y)$, which is the output of the algorithm. By using this algorithm, a phase pattern $P_1(x,y)$ can be acquired. The algorithm can be completed within half an hour by a common desktop computer.

Surface Topography of the Printed Patterns. A phase pattern is calculated and loaded on the SLM, then a tilted intermediate image can be formed. The final image is formed at the interface between the glass slide and the prepolymer solution. We used poly(ethelene glycol) diacrylate (PEGDA, Mn = 575) mixed with 1% Irgacure 819 photoinitiator as the prepolymer material. After a few seconds' exposure, ultrathin polymer patterns are formed on the glass slide.

Then we used the optical profiler to measure the surface topography of the patterns. Figure 4a and b show the topographies of a "smiling face". Figure 4c and d show the topography of a "honeycomb". Figure 4e and f show the topographies of a "UCSD" pattern. The thickness of these patterns are around 200 nm.

DOI: 10.1021/acsami.9b02728
ACS Appl. Mater. Interfaces 2019, 11, 16059−16064

CONCLUSIONS

We have developed a new method that utilizes the patterned evanescent field to create arbitrary structures with nanoscale thickness control without using spin-coating to control the thickness or using a physical photomask for patterning. The phase-only SLM can generate an image that coincides with the TIR interface and prints the structures in a projection fashion. We have demonstrated that arbitrary ultrathin structures as thin as 200 nm can be achieved. However, its lateral resolution is theoretically limited by the diffraction limit. Because this setup requires a relatively long working distance, a high numerical aperture (NA) objective lens cannot be used. Thus, the lateral resolution is limited to a few micrometers. Due to the aberrations, we could only demonstrate a 20 μm feature size. In order to make the image in-focus on the entire TIR interface, the image plane should not be perpendicular to the light incident direction. The tilted image is generated by the holography method in this work for proof-of-concept purpose. However, the holography method requires an expensive coherent light source. Calculating the phase pattern by the 3D-MRAF algorithm is time-consuming. In practice, it is more favorable to use a tilted lens combined with a digital mirror device (DMD) to pattern the light field. Although the tilted lens needs to be specially designed, better image quality can be achieved, and it does not need the time-consuming algorithm.

Currently two-photon polymerization method is the most popular nanoscale 3D fabrication technique. Although it features extremely fine resolution, its fabrication speed is very slow due to the point-scanning nature.[3] On the other hand, light-projection-based 3D printing methods are facing the bottleneck of poor axial resolution. We expect this evanescent field patterning concept can be applied to light-projection-based 3D printing in the future,[6] offering a fast fabrication speed, submicrometer axial resolution, and micrometer-scale lateral resolution.

METHODS

Materias. DPPA was purchased from Sartomer. Irgacure 819 was purchased from Ciba Specialty Chemicals, which is now acquired by BASF. PEGDA was purchased from Sigma-Aldrich. CH_2I_2 was purchased from Alfa Aesar. N-SF11 equilateral prism was purchased from Edmund Optics. N-SF11 glass slide was purchased from Volume Precision Glass.

Equipment. The SLM is Holoeye Pluto. The SEM is Zeiss Sigma 500. The optical profiler is Veeco NT1100. The sputter coater is Emitech K575X.

Sample characterization: Samples for SEM imaging were sputter coated by iridium, then were imaged under 2 kV voltage. Samples for optical profiler were imaged without coating. Due to the limitation of the optical profiler which uses white light interference to detect the height profile, height values at steep edges are not able to be detected. In order to make a complete topography, these "bad pixels" are replaced with the average of their surrounding "good pixels". This processing was performed with Matlab.

Software Program. The program of the 3D-MRAF algorithm was developed by the authors. This program runs in the Matlab environment. The light filed is represented by a 1080 × 1920 × 128 matrix, thus a computer of 32GB memory can handle this program.

AUTHOR INFORMATION

Corresponding Author

*E-mail: chen168@eng.ucsd.edu.

ORCID

Shangting You: 0000-0001-6937-5327
Wei Zhu: 0000-0002-2524-0866
Pengrui Wang: 0000-0001-9185-2951

Author Contributions

The manuscript was written through contributions of all authors. All authors have given approval to the final version of the manuscript.

Notes

The authors declare no competing financial interest.

ACKNOWLEDGMENTS

This work was supported in part by National Institutes of Health (R21AR074763, R01EB021857) and National Science Foundation (CMMI-1547005 and CMMI-1644967). Part of the work is performed at San Diego Nanotechnology Infrastructure (SDNI) of UC San Diego, a member of the National Nanotechnology Coordinated Infrastructure (NNCI), which is supported by the National Science Foundation (Grant ECCS-1542148).

ABBREVIATIONS

TIR = total internal reflection
TIRFM = total internal reflection fluorescence microscopy
ATR-IR = attenuated total reflection infrared spectroscopy
SLM = spatial light modulator
MRAF = mixed-region amplitude freedom
DPPA = dipentaerythritol pentaacrylate
SEM = scanning electron microscopy
GS = Gerchberg−Saxton
AA = adaptive-additive
CGH = computer-generated holography
PEGDA = poly(ethelene glycol) diacrylate
DMD = digital micromirror device

REFERENCES

(1) Madou, M. J. *Manufacturing Techniques for Microfabrication and Nanotechnology*; CRC Press, 2011.
(2) Lu, Y.; Chen, S. C. Micro and Nano-Fabrication of Biodegradable Polymers for Drug Delivery. *Adv. Drug Delivery Rev.* **2004**, *56* (11), 1621−1633.
(3) You, S.; Li, J.; Zhu, W.; Yu, C.; Mei, D.; Chen, S. Nanoscale 3D Printing of Hydrogels for Cellular Tissue Engineering. *J. Mater. Chem. B* **2018**, *6* (15), 2187−2197.
(4) Tumbleston, J. R.; Shirvanyants, D.; Ermoshkin, N.; Janusziewicz, R.; Johnson, A. R.; Kelly, D.; Chen, K.; Pinschmidt, R.; Rolland, J. P.; Ermoshkin, A.; Samulski, E. T.; DeSimone, J. M. Continuous Liquid Interface Production of 3D Objects. *Science* **2015**, *347* (6228), 1349−1352.
(5) Zhang, A. P.; Qu, X.; Soman, P.; Hribar, K. C.; Lee, J. W.; Chen, S.; He, S. Rapid Fabrication of Complex 3D Extracellular Microenvironments by Dynamic Optical Projection Stereolithography. *Adv. Mater.* **2012**, *24* (31), 4266−4270.
(6) Lu, B.; Lan, H.; Liu, H. Additive Manufacturing Frontier: 3D Printing Electronics. *Opto-Electron. Adv.* **2018**, *1* (1), 17000401−17000410.
(7) Hwang, H. H.; Zhu, W.; Victorine, G.; Lawrence, N.; Chen, S. 3D-Printing of Functional Biomedical Microdevices via Light-and Extrusion-Based Approaches. *Small Methods.* **2018**, *2* (2), 1700277.
(8) Melchels, F. P. W.; Feijen, J.; Grijpma, D. W. A Review on Stereolithography and Its Applications in Biomedical Engineering. *Biomaterials* **2010**, *31* (24), 6121−6130.

DOI: 10.1021/acsami.9b02728
ACS Appl. Mater. Interfaces 2019, 11, 16059−16064

(9) Zhu, W.; Ma, X.; Gou, M.; Mei, D.; Zhang, K.; Chen, S. 3D Printing of Functional Biomaterials for Tissue Engineering. *Curr. Opin. Biotechnol.* **2016**, *40*, 103−112.
(10) Born, M.; Wolf, E. *Principles of Optics: Electromagnetic Theory of Propagation, Interference and Diffraction of Light*; Elsevier, 2013.
(11) Fish, K. N. Total Internal Reflection Fluorescence (TIRF) Microscopy. *Curr. Protoc. Cytom.* **2009**, *50* (1), 12.18.1−12.18.13.
(12) G. Kazarian, S.; Andrew Chan, K. L. ATR-FTIR Spectroscopic Imaging: Recent Advances and Applications to Biological Systems. *Analyst* **2013**, *138* (7), 1940−1951.
(13) Chua, J. K.; Murukeshan, V. M.; Tan, S. K.; Lin, Q. Y. Four Beams Evanescent Waves Interference Lithography for Patterning of Two Dimensional Features. *Opt. Express* **2007**, *15* (6), 3437−3451.
(14) Martinez-Anton, J. C. Surface Relief Subwavelength Gratings by Means of Total Internal Reflection Evanescent Wave Interference Lithography. *J. Opt. A: Pure Appl. Opt.* **2006**, *8* (4), S213.
(15) Ecoffet, C.; Espanet, A.; Lougnot, D. J. Photopolymerization by Evanescent Waves: A New Method to Obtain Nanoparts. *Adv. Mater.* **1998**, *10* (5), 411−414.
(16) Zhou, Y.; Hong, M. H.; Fuh, J. Y. H.; Lu, L.; Lukiyanchuk, B. S. Evanescent Wave Interference Lithography for Surface Nano-Structuring. *Phys. Scr.* **2007**, *T129*, 35−37.
(17) Guo, X.; Du, J.; Guo, Y.; Yao, J. Large-Area Surface-Plasmon Polariton Interference Lithography. *Opt. Lett.* **2006**, *31* (17), 2613−2615.
(18) Kong, W.; Du, W.; Liu, K.; Wang, C.; Liu, L.; Zhao, Z.; Luo, X. Launching Deep Subwavelength Bulk Plasmon Polaritons through Hyperbolic Metamaterials for Surface Imaging with a Tuneable Ultra-Short Illumination Depth. *Nanoscale* **2016**, *8* (38), 17030−17038.
(19) Liu, L.; Liu, K.; Zhao, Z.; Wang, C.; Gao, P.; Luo, X. Sub-Diffraction Demagnification Imaging Lithography by Hyperlens with Plasmonic Reflector Layer. *RSC Adv.* **2016**, *6* (98), 95973−95978.
(20) Lin, Y.; Hong, M. H.; Chong, T. C.; Lim, C. S.; Chen, G. X.; Tan, L. S.; Wang, Z. B.; Shi, L. P. Ultrafast-Laser-Induced Parallel Phase-Change Nanolithography. *Appl. Phys. Lett.* **2006**, *89* (4), 041108.
(21) Pasienski, M.; DeMarco, B. A High-Accuracy Algorithm for Designing Arbitrary Holographic Atom Traps. *Opt. Express* **2008**, *16* (3), 2176−2190.
(22) Campo, A. del; Greiner, C. SU-8: A Photoresist for High-Aspect-Ratio and 3D Submicron Lithography. *J. Micromech. Microeng.* **2007**, *17* (6), R81−R95.
(23) Laskar, J. M.; Shravan Kumar, P.; Herminghaus, S.; Daniels, K. E.; Schröter, M. High Refractive Index Immersion Liquid for Superresolution 3D Imaging Using Sapphire-Based Aplanatic Numerical Aperture Increasing Lens Optics. *Appl. Opt.* **2016**, *55* (12), 3165.
(24) Merklinger, H. M. *Focusing the View Camera: A Scientific Way to Focus the View Camera and Estimate Depth of Field*; H.M. Merklinger: Ottawa, Ontario, Canada, 1993.
(25) Bruce, G. D.; Mayoh, J.; Smirne, G.; Torralbo-Campo, L.; Cassettari, D. A Smooth, Holographically Generated Ring Trap for the Investigation of Superfluidity in Ultracold Atoms. *Phys. Scr.* **2011**, *2011* (T143), 014008.
(26) Yang, G.; Dong, B.; Gu, B.; Zhuang, J.; Ersoy, O. K. Gerchberg-Saxton and Yang-Gu Algorithms for Phase Retrieval in a Nonunitary Transform System: A Comparison. *Appl. Opt.* **1994**, *33* (2), 209−218.
(27) You, S.; Kuang, C.; Toussaint, K. C.; Zhou, R.; Xia, X.; Liu, X. Iterative Phase-Retrieval Method for Generating Stereo Array of Polarization-Controlled Focal Spots. *Opt. Lett.* **2015**, *40* (15), 3532.
(28) Kotlyar, V. V.; Seraphimovich, P. G.; Soifer, V. A. An Iterative Algorithm for Designing Diffractive Optical Elements with Regularization. *Opt. Lasers Eng.* **1998**, *29* (4−5), 261−268.
(29) Soifer, V. A. *Methods for Computer Design of Diffractive Optical Elements*; John Wiley & Sons, Inc., 2001.
(30) Whyte, G.; Courtial, J. Experimental Demonstration of Holographic Three-Dimensional Light Shaping Using a Gerchberg-Saxton Algorithm. *New J. Phys.* **2005**, *7* (1), 117.
(31) Zhang, C.; Hu, Y.; Li, J.; Lao, Z.; Ni, J.; Chu, J.; Huang, W.; Wu, D. An Improved Multi-Exposure Approach for High Quality Holographic Femtosecond Laser Patterning. *Appl. Phys. Lett.* **2014**, *105* (22), 221104.
(32) Shabtay, G. Three-Dimensional Beam Forming and Ewald's Surfaces. *Opt. Commun.* **2003**, *226* (1−6), 33−37.

DOI: 10.1021/acsami.9b02728
ACS Appl. Mater. Interfaces 2019, 11, 16059−16064